Fracture Toughness Behavior of Ex-Service 2-1/4Cr-1Mo Steels from a 22-Year-old Fossil Power Plant

P.K. LIAW, M.G. BURKE, A. SAXENA, and J.D. LANDES

Elevated-temperature fracture toughness properties were developed on ex-service 2-1/4Cr-1Mo steel weldments. Fracture toughness was measured on both base and heat-affected zone (HAZ) metals. A composite specimen consisting of base, HAZ, and weld metals was used to develop fracture toughness properties in the HAZ area. It was observed that the *J-R* curve of the HAZ was significantly lower than that of the base metal. Increasing crack extension increased the difference between the *J-R* curves of the base metal and the HAZ. Dimpled fracture was the prime fracture mode in the base metal specimen, and a mixed-mode (ductile and "granular") fracture was found in the HAZ specimens. Scanning transmission electron microscopy (STEM) examination revealed significant intergranular carbide precipitation and agglomeration within the HAZ. The lower fracture toughness of the HAZ, as compared to the base metal, was attributed to the large accumulation of carbides in the grain boundaries of the HAZ, which weakened the grain boundaries and caused "granular" fracture.

I. INTRODUCTION

REMAINING life prediction has recently become an issue in the power generation industry.[1–9] The interest in the area of remaining life prediction arises from the necessity to avoid costly forced outages, safety considerations, and the need to extend the operating life of structural components beyond the original design life.[1–4] In fossil fuel power generation systems, many structural components, such as steam pipes and headers, high-pressure steam turbine rotors, and casings, operate at high temperatures. While there is an industrial need for the development of a life prediction methodology for these components, in order to be accurate, this methodology must incorporate the appropriate elevated-temperature failure mechanisms.

Recently, a remaining crack growth life prediction methodology for high-temperature structural components was developed[1,8,9] in which the final life of the component was determined by fracture toughness. Therefore, fracture toughness properties in ex-service materials are of considerable importance. Usually, fracture toughness data were obtained on virgin materials which have not experienced in-service operation. Little work has been conducted to characterize fracture toughness behavior of in-service or ex-service materials. Because of the long-term, elevated-temperature operation, the fracture characteristics of an in-service (or ex-service) material may be significantly different from that of a corresponding virgin material.[6,10,11,12] Thus, the consideration of service history is important in selecting fracture toughness values for life prediction analyses.

Potentially, failure of elevated-temperature components can result from creep or creep-fatigue crack growth associated with pre-existing fabrication defects or inclusions or service-initiated defects. Also, high-temperature components are prone to cracking along the heat-affected zone (HAZ) areas where weld defects can be present, as shown by higher crack growth rates and lower fracture resistance along HAZ regions.[8,9] Thus, the fracture behavior in the HAZ regions needs to be emphasized for life prediction.

In this investigation, the fracture toughness behavior of a 2-1/4Cr-1Mo steel weldment and corresponding base metal samples from ex-service superheater headers are characterized. Extensive microstructural characterization was performed to further understand the fracture characteristics of these steel weldments.

P.K. LIAW, Fellow Engineer, and M.G. BURKE, Senior Engineer, are with Department of Materials Evaluation, Westinghouse Science and Technology Center, Pittsburgh, PA 15235. A. SAXENA, Professor, is with School of Materials Engineering, Georgia Institute of Technology, Atlanta, GA 30332. J.D. LANDES, Professor, is with Department of Engineering Science and Mechanics, The University of Tennessee, Knoxville, TN 37996-2030.

Manuscript submitted August 8, 1989.

II. EXPERIMENTAL PROCEDURE

A. *Material*

The chemical compositions of the 2-1/4Cr-1Mo steel investigated in this study are presented in Table I. The 2-1/4Cr-1Mo steel was from a Penelec's Shawville #3 superheater outlet header, which was retired after 22 years of service.[13] The Shawville header was 508 mm in diameter, with a wall thickness of 111 mm, and the length was 14 m. A longitudinal seam weld ran along the length direction of the 2-1/4Cr-1Mo header. The end of the header labeled as the north end (also called the hot region or hot end) experienced a higher service temperature, compared to the end labeled as the south end (also called the cold region or cold end). The estimated service temperatures of the hot and cold regions were 579 °C and 546 °C for the 2-1/4Cr-1Mo header, respectively.

Sample plates for mechanical testing were machined from both hot and cold regions of each header. The designations of sample plates are shown in Table II. Note that some samples were taken from the weldment regions which contained both base and weld metals.

B. *Microstructural Characterization*

1. *Metallography*

Conventional optical metallography of samples taken from the 2-1/4Cr-1Mo header was conducted to reveal

Table I. Chemical Compositions of 2-1/4Cr-1Mo Steel (in Weight Percent)

Material	C	Mn	P	S	Si	Cr	Mo	Cu	Sn	Pb	Al	Fe
2-1/4Cr-1Mo	0.102	0.47	0.006	0.018	0.20	2.22	1.01	0.014	0.039	0.001	<0.01	bal.

the microstructures. Microhardness tests were performed on the 2-1/4Cr-1Mo steel weldment to examine the hardness levels in the base, HAZ, and weld metals.

2. *Scanning transmission electron microscopy*

Thin-foil specimens were prepared from the base and HAZ regions of the weldment by conventional electropolishing techniques. Transmission electron microscopy (TEM) and limited scanning electron microscopy (SEM) were performed using a Philips* EM400T analytical electron microscope operated at 120 kV. Transmission electron microscopy/scanning transmission electron microscopy (STEM) was employed in order to identify the carbides present in the steels, to determine the extent of carbide precipitation, and to evaluate the general microstructures. Scanning electron microscopy was used to supplement the TEM/STEM microstructural data by providing information concerning the general carbide distribution throughout the steel.

*PHILIPS is a trademark of Philips Electronic Instruments Corporation, Mahwah, NJ.

C. *Tensile Tests*

The geometry of a tensile test specimen is shown in Figure 1(a). The gage length was 25.4 mm and the diameter 3.81 mm. The specimens were machined from both hot and cold regions of the header.

Two kinds of tensile specimens were obtained from the test materials. The first kind was a composite specimen whose gage length section consisted of base, HAZ, and weld metals. The HAZ area was in the middle of the gage length section of the specimen, and the HAZ plane was approximately perpendicular to the loading direction. The composite specimen represented the overall behavior of a weldment. The second type of test specimen was a base metal sample, the entire section of which was from the base metal region. The second type of specimen was used to obtain tensile properties of the base metal.

Tensile tests were performed at −40 °C and 593 °C for the 2-1/4Cr-1Mo steel. For elevated-temperature testing, the tensile specimen was heated to the desired temperature in a resistance-type furnace. The specimen temperature in the gage length section was controlled within ±2 °C of the prescribed test temperature. For −40 °C temperature testing, the specimen was enclosed in a chamber where liquid nitrogen constantly flowed in from a supply tank and surrounded the gage length section. The test temperature was maintained by controlling the flow rate of liquid nitrogen. Note that the 593 °C test was conducted in ambient air.

Tensile tests were performed at a strain rate of 0.05 per minute. Complete stress *vs* strain curves were obtained by measuring the strain in the gage length section of the tensile specimen using an extensometer attached to the specimen. The values of yield strength, ultimate tensile strength, elongation, and reduction in area were determined. Duplicate tests were conducted to ensure the reproducibility of test results. The engineering stress (S) and engineering strain (e) were converted into the true stress (σ) and true strain (ε) using the following equations:

$$\sigma = S(1 + e)$$

$$\varepsilon = \ln (1 + e)$$

Table II. Sample Designation

Designation	Steel	Location	Metal
WHB	2-1/4Cr-1Mo	hot region	base
WCB	2-1/4Cr-1Mo	cold region	base
WCW	2-1/4Cr-1Mo	cold region	weldment (base + weld)

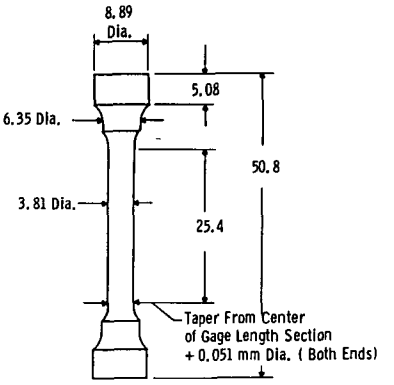

(*a*)

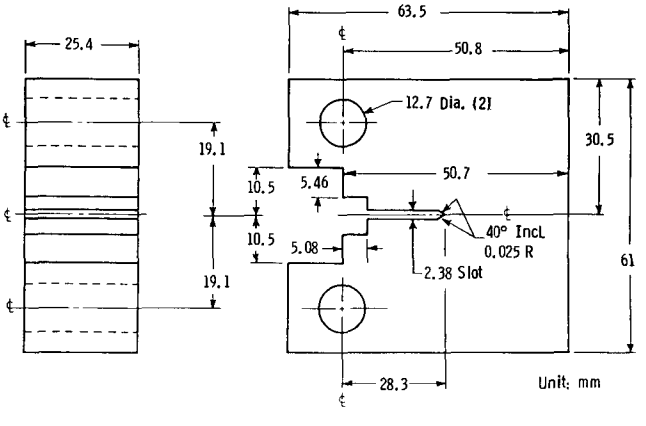

(*b*)

Fig. 1—Specimen geometry. (*a*) Tensile specimen and (*b*) fracture toughness specimen.

The developed true stress (σ)-true strain (ε) curves were fitted to the following equation:

$$\varepsilon = \frac{\sigma}{E} + D\sigma^m$$

where E is Young's modulus, and D and m are the plasticity coefficient and exponent, respectively.

D. *Fracture Toughness Tests*

The specimen geometry for fracture toughness tests is shown in Figure 1(b). The test specimen was a compact (CT) specimen, 50.8-mm wide (W), 61-mm high ($2H$), and 25.4-mm thick (B). The ratio of machine notch depth, a_m (28.3 mm), to specimen width was 0.55 for the CT specimen. Test specimens were machined from both hot and cold regions of the headers.

Two types of CT specimens were also fabricated for fracture toughness testing, which included the composite specimens and the base metal specimens. The composite specimens contained the base, HAZ, and weld metal regions. The cracking plane in these specimens was approximately aligned with the HAZ area, and thus, representative fracture toughness properties in the HAZ region were developed. The base metal specimens were machined entirely from the base metal regions of the header. These specimens were in the circumferential-longitudinal (CL) orientation.[14]

Fracture toughness tests were conducted at the two temperatures of −40 °C and 593 °C for the 2-1/4Cr-1Mo steel. These test temperatures were identical to those used during tensile testing, and the test setups were also identical.

Fracture toughness tests were performed in accordance with the ASTM Standard E813-87, "Test Method for J_{IC}, A Measure of Fracture Toughness."[15] Prior to fracture toughness testing, the CT specimens were fatigue-precracked at room temperature to ensure that a sharp crack was present in front of the machine notch. The precrack length (a_f) was equal to approximately 2 mm. Thus, the ratio of crack length ($a_0 = a_m + a_f$) to specimen width (W) for the CT specimen was approximately 0.6. Following precracking, the specimens were side-grooved 10 pct on each side to ensure a uniform crack front during stable crack growth.

Fracture toughness properties were determined in the J-R curve format, and J_{IC} was evaluated using the elastic unloading compliance test method.[15–18] Briefly, a clip gage was mounted on the load line of the CT specimen to measure load *vs* crack opening displacement. During the fracture toughness testing, the specimens were periodically unloaded 10 pct of the maximum load to develop elastic unloading lines (*i.e.*, the elastic unloading load-displacement lines). The slope of the elastic unloading line is related through a compliance calibration to the specimen stiffness and the crack length. The change in the slopes between subsequent "unloading compliance" lines, therefore, was used to calculate the change in crack length during the progress of the test. This procedure results in an instantaneous measure of crack size which is also used to calculate the value of the J-integral using the method outlined in Reference 17. Thus, J-R curves were generated where J was plotted *vs* crack extension or growth (Δa). Note that the value of Δa equals crack extension beyond the precrack. Duplicate tests were performed to ensure reproducibility in the test data.

E. *Fractography*

After fracture toughness testing, fracture surfaces were carefully examined by using SEM. Since some of the tests were conducted at elevated temperatures, heavy oxide deposits were found to be present on the fracture surfaces. Therefore, prior to SEM observations, the fracture surfaces were electrochemically cleaned in an ENDOX* solution[19] and ultrasonically rinsed in methanol to remove oxide debris.

*ENDOX is a trademark of Ethone, Inc., West Haven, CT.

III. RESULTS AND DISCUSSION

A. *Metallography and Hardness*

1. *Grain structure*

The microstructures of the 2-1/4Cr-1Mo steel are presented in Figures 2(a) and (b), respectively. Figure 2(a) shows the microstructures of the base metal and HAZ in the cold region of the 2-1/4Cr-1Mo header, while Figure 2(b) presents the microstructure of the base metal from the hot region. The grain size of the base metal (cold region) was found to be significantly greater than that of the HAZ (cold region). However, the grain size of the base metal in the hot region was greater than that of the base metal in the cold region. The grain sizes of the base metal (cold region), the HAZ (cold region), and the base metal (hot region) were ASTM #9, 12, and 6, respectively.

2. *Hardness*

Measurements of microhardness were taken across the HAZ area, and the results are presented in Figure 3 for the 2-1/4Cr-1Mo steel weldment. The hardness level in the HAZ area was found to be generally greater than that in the base or weld metal regions. This observation seemed to be consistent with the grain size measurement, which showed smaller grain size in the HAZ than in the base metal. Furthermore, the base metal had lower hardness levels than the weld metal.

The hardnesses of the hot and cold regions of the 2-1/4Cr-1Mo steel were also measured and compared on the Rockwell B scale. The hardnesses of the hot and cold regions were 66 to 67, and 90 to 93 Rockwell B, respectively. The significantly lower hardness in the hot region of the 2-1/4Cr-1Mo steel, compared to the cold region, may be due, in part, to the larger grain size in the hot region (Figure 2).

B. *Scanning Transmission Electron Microscopy*

The microstructure of the HAZ was also characterized by a very fine-grained ferrite with coarse agglomerated carbides which heavily decorated the grain boundaries. Figure 4 illustrates the extent of the carbide coverage along ferrite grain boundaries. In this STEM/SEM set of micrographs, the carbides are clearly evident at the boundaries. In particular, one very coarse agglomerated

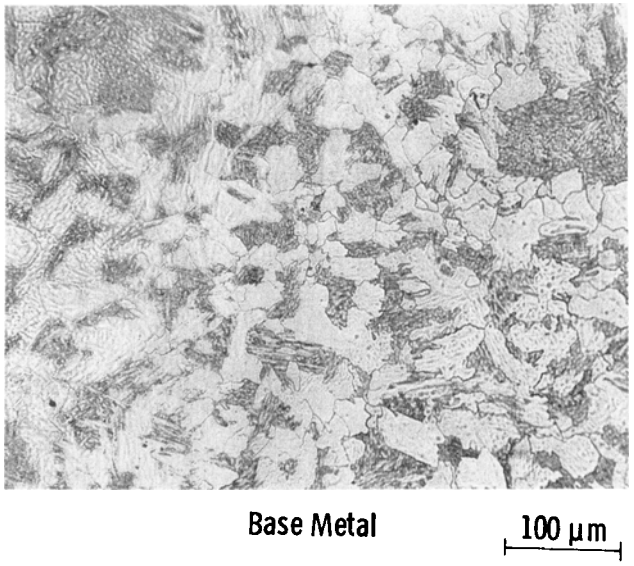

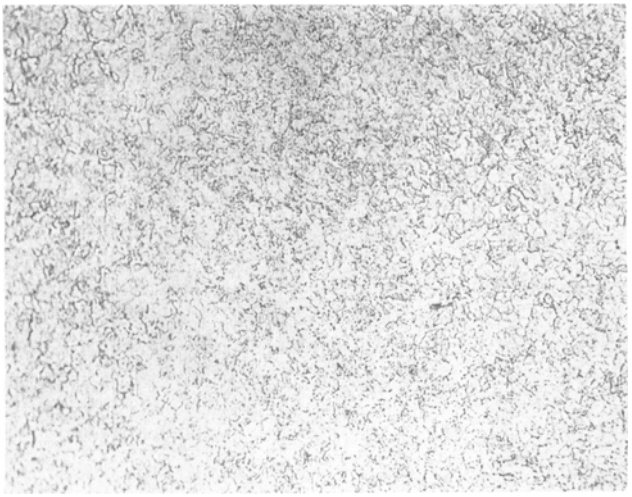

Fig. 2—Microstructures of 2-1/4Cr-1Mo steel weldment (WCW) from (*a*) cold region and (*b*) hot region.

carbide which extends along the entire boundary (arrowed) can be observed. The TEM micrographs in Figure 5 further depict the agglomerated carbide morphologies present along the grain boundaries of the HAZ. Numerous dislocation networks were also observed in the HAZ, indicating that extensive polygonization had occurred during elevated-temperature service exposure. The carbides were identified as $M_{23}C_6$, M_6C, and M_7C_3 by electron diffraction (Figures 5(c) and (d)).

Unlike the HAZ metal, the base metal had a coarse ferrite grain size. Detailed examination of the base metal revealed that some carbide agglomeration had occurred along segments of the ferrite grain boundaries (Figures 6 and 7). The STEM and corresponding SEM micrographs (Figure 6) of the base metal illustrate the extent of intergranular carbide precipitation observed in this material. The nonuniform distribution of intergranular carbides is clearly shown in Figures 6(a) and (b). Moreover, the SEM micrographs in Figures 7(a) and (b) exhibit the general carbide distribution observed in the base metal. The distribution of intragranular carbides was found to be inhomogeneous, as shown in Figure 7. Because of this nature of inhomogeneity, clusters of carbides (arrowed) were readily evident (Figure 7(a)). Electron diffraction confirmed that these carbides were $M_{23}C_6$, M_6C, and M_7C_3.

Nonuniform intragranular precipitation of Mo_2C was also observed in the base metal. These needlelike carbides were approximately 0.5 microns in length. Electron diffraction analyses showed that the Mo_2C carbides were aligned along ⟨100⟩ directions in the ferrite (Figure 8). In addition to the Mo_2C precipitation, regions of coarse intragranular carbides were observed in the base metal (Figure 7). Also, the morphology of some carbides resembled a degenerate pearlitic structure (Figure 7(c)). Such features were inhomogeneously distributed throughout the base metal in both hot and cold regions of the header.

The proportion of intragranular carbides in the base metal was much greater than that in the HAZ metal (Figures 4 through 8). From the STEM observations, it appears that more agglomerated intergranular carbides are present in the HAZ metal, as compared to the base metal (Figures 4, 5, and 7). Furthermore, the carbide coverage along the grain boundaries of the HAZ metal was more extensive than that in the base metal.

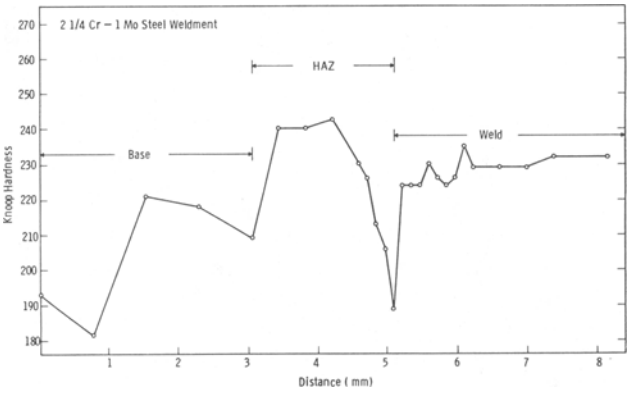

Fig. 3—Hardness profile of 2-1/4Cr-1Mo steel weldment (cold region).

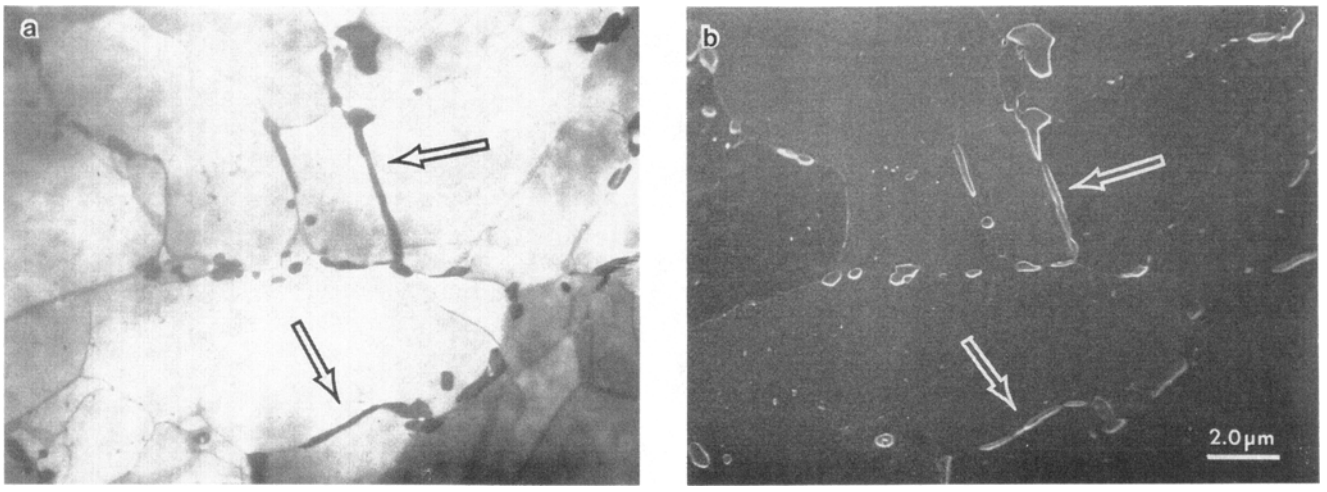

Fig. 4—(*a*) STEM and (*b*) complementary SEM micrographs illustrating the extent of intergranular precipitation in the 2-1/4Cr-1Mo HAZ metal. Note the coarse agglomerated carbides (arrowed) which extend along a very large proportion of the grain boundaries.

The microstructures observed in the present ex-service 2-1/4Cr-1Mo steel were substantially different from the typical quenched and tempered structure which was not exposed to service. For comparison purposes, the microstructure of a typical quenched and tempered 2-1/4Cr-1Mo steel[20] is presented in Figure 9. The typical precipitates present after tempering included M_3C, Mo_2C, and M_7C_3, with $M_{23}C_6$ and M_6C forming after prolonged tempering. Therefore, the presence of $M_{23}C_6$ and M_6C carbides observed in the ex-service 2-1/4Cr-1Mo steel confirmed

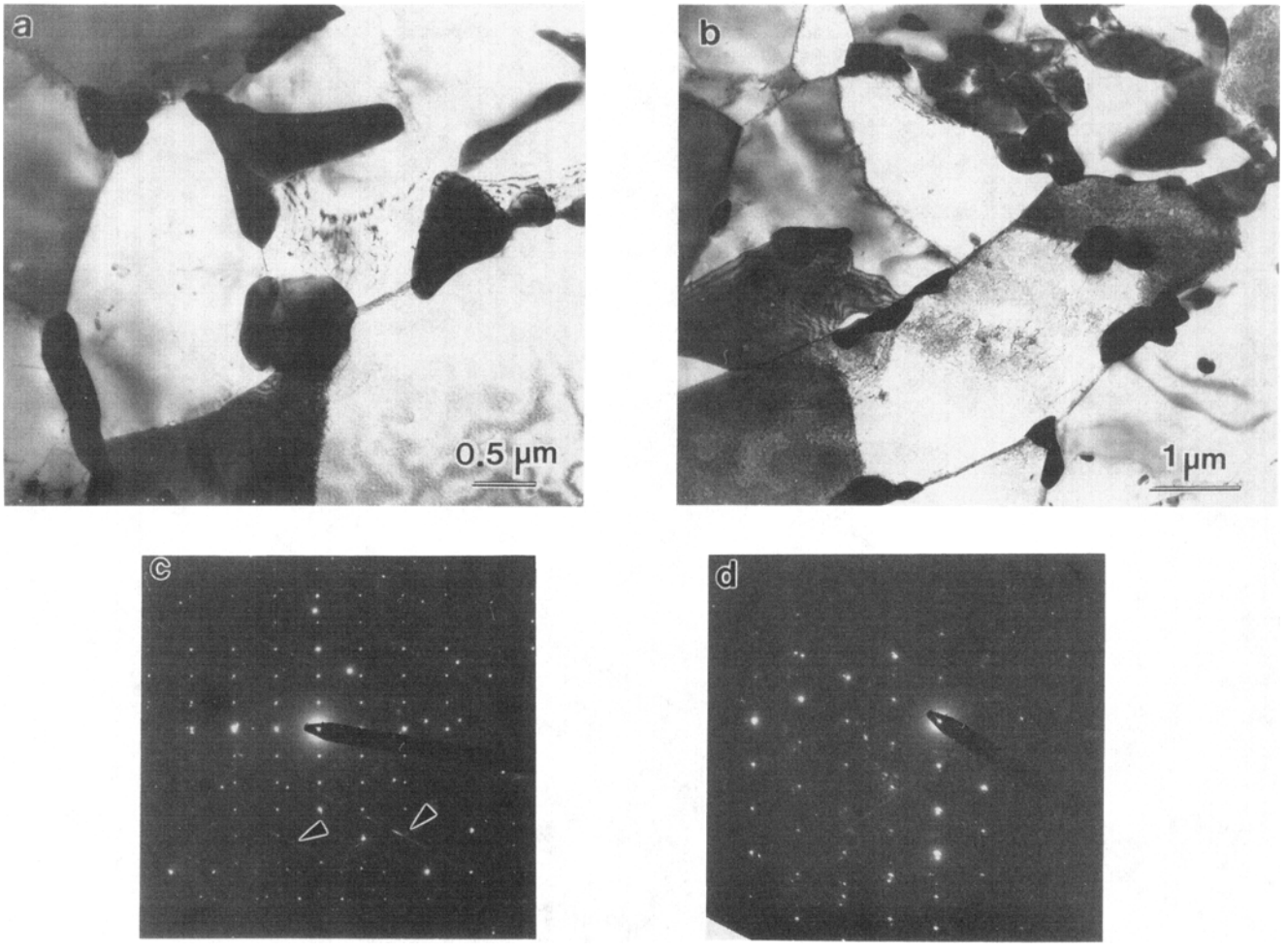

Fig. 5—(*a*) and (*b*) TEM micrographs of the coarse intergranular carbides observed in the HAZ metal of the 2-1/4Cr-1Mo steel. (*c*) [112] electron diffraction pattern from an M_6C carbide. The faint streaks (arrowed) are from an M_7C_3 carbide. (*d*) [114] electron diffraction pattern obtained from a coarse $M_{23}C_6$ carbide.

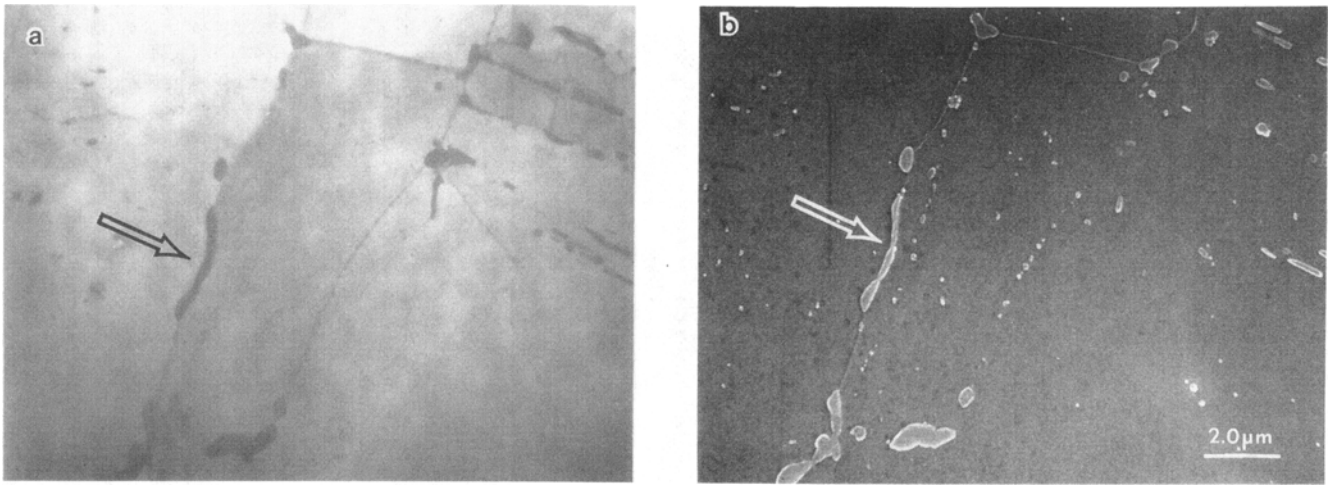

Fig. 6—(*a*) STEM and (*b*) complementary SEM micrographs which depict the variation in the distribution of carbides along ferrite grain boundaries in the 2-1/4Cr-1Mo base metal. Note the presence of both agglomerated (arrowed) and discrete carbide precipitates.

that these steels have experienced extensive thermal aging at elevated temperatures.

The sizes of the carbides in the present ex-service 2-1/4Cr-1Mo steel (Figures 4 through 8) were significantly larger than those in a typical quenched and tempered steel (Figure 9). Moreover, the ex-service steel was characterized by considerable carbide agglomeration and decoration of grain boundaries as compared with a quenched and tempered structure. Thus, the long service time promoted extensive carbide growth and coalescence

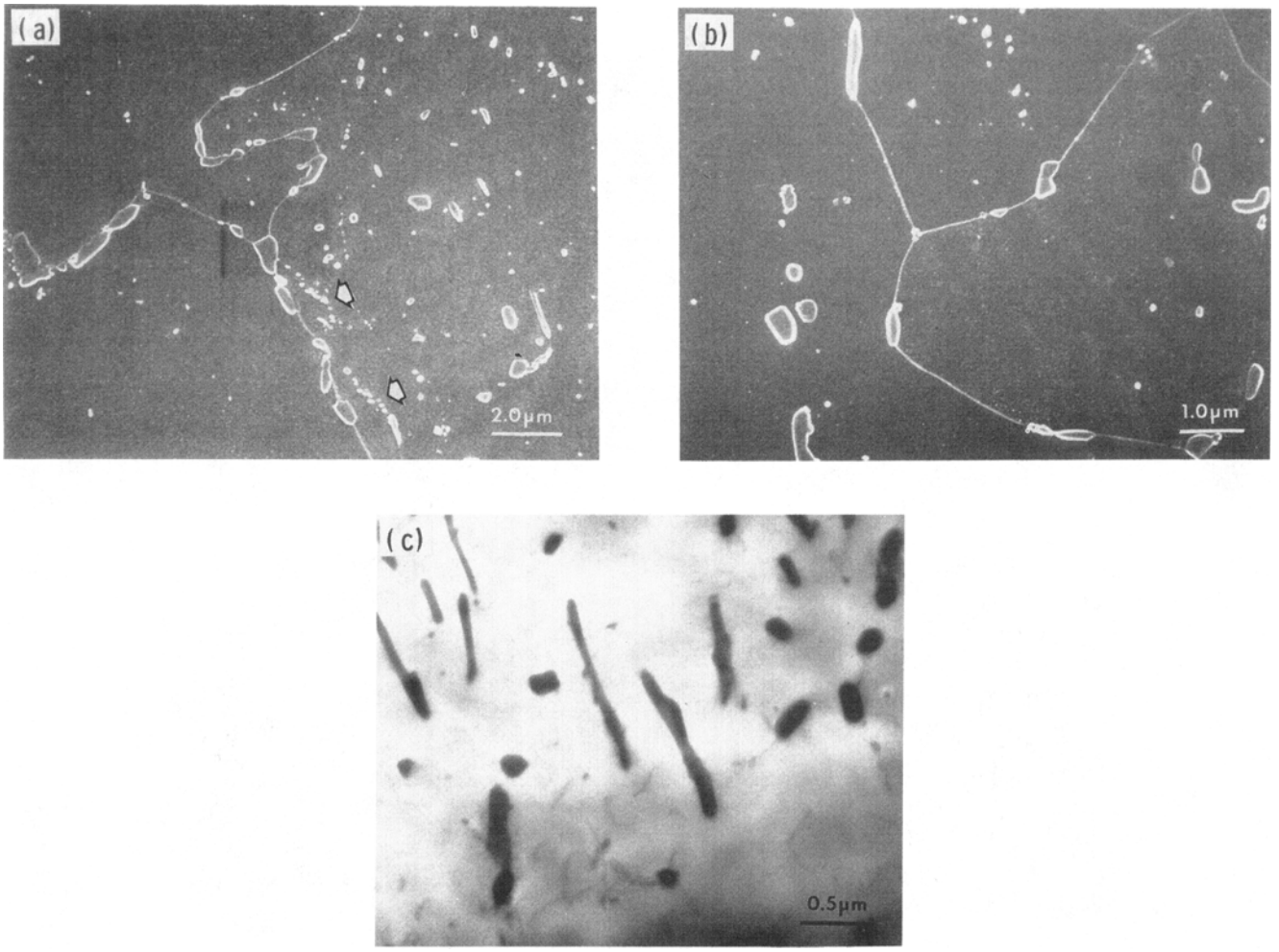

Fig. 7—(*a*) and (*b*) SEM micrographs of the 2-1/4Cr-1Mo base metal which show the general carbide distribution in the material. (*c*) STEM micrograph showing degenerate pearlite morphology of intragranular carbides observed in the 2-1/4Cr-1Mo base metal.

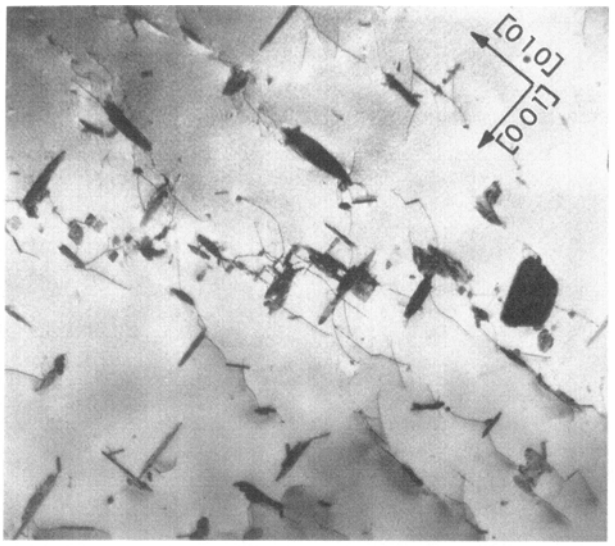

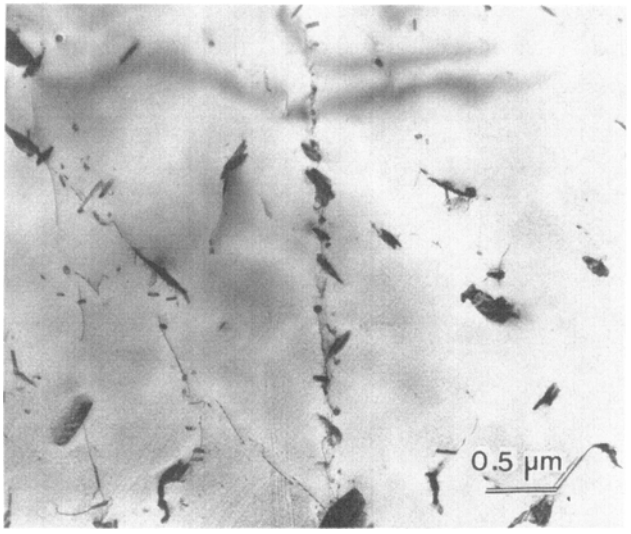

Fig. 8—TEM micrographs of intragranular Mo_2C precipitates observed in the 2-1/4Cr-1Mo base metal.

both within the matrix and along the grain boundaries. Such coalescence and agglomeration resulted in extensive carbide coverage of the grain boundaries of ex-service steels.

C. *Tensile Properties*

The results of tensile tests of the 2-1/4Cr-1Mo steel are listed in Table III. The composite specimens containing the HAZ area in the center of the test section are identified as HAZ in the "material type" column of each table. There is good reproducibility of the results from the two tests conducted for each condition.

At 593 °C, the average values of yield strength in the hot and cold regions of the base metal and the HAZ in the cold region were 131, 105, and 119 MPa, respectively. At −40 °C, the average yield strength of the base metal (cold region) was 203 MPa. The yield strength at 593 °C of the base metal in the hot region was greater than that in the cold region. The yield strength of the

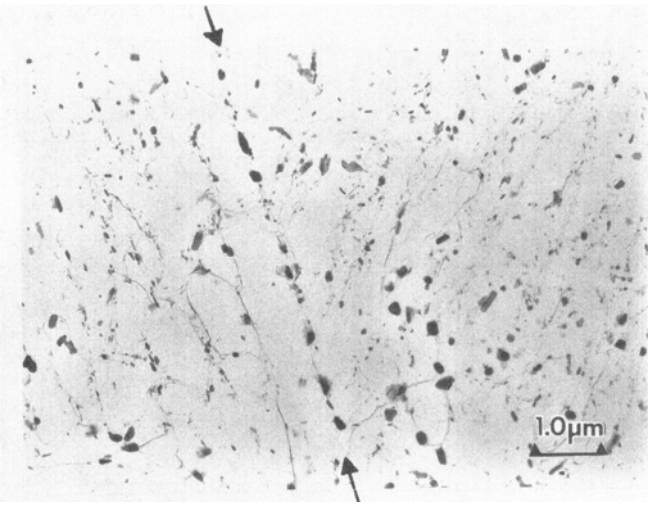

Fig. 9—TEM micrograph (carbon extraction replica) of a typical 2-1/4Cr-1Mo base metal in the quenched and tempered condition. Note the extensive precipitation of fine carbides along the martensite lath boundaries and prior austenite grain boundary (arrowed).

HAZ (cold region) was slightly greater than that of the base metal from the cold region, and the percent elongation was lower. In the base metal (cold region), the yield strength at 593 °C was found to be lower than that at −40 °C. The values of D and m are presented in Table III.

D. *Fracture Toughness Behavior*

1. *J-R curves*

The *J-R* curves from the various regions of the 2-1/4Cr-1Mo steel are shown in Figure 10. The results shown include test data from duplicate specimens. A reasonably good agreement in the *J-R* curves of the duplicate tests was observed for the base metal in the hot region. However, some variability in the *J-R* curves was found for the two tests from the base metal in the cold region and those in the HAZ. The reason for the variability in these specimens is discussed later in the paper. The base metals taken from hot and cold regions seemed to exhibit comparable *J-R* curves, although one *J-R* curve of the base metal (cold region) was found to be elevated, relative to the other curves.

The *J-R* curves of the base metals were significantly higher than those of the HAZ, and the difference increased with crack extension. At −40 °C, the extent of stable crack growth was negligible, and the fracture behavior was dominated by cleavage. Therefore, no *J-R* curves are reported at this temperature.

The fracture toughness properties in the weld and the fusion line (the base metal/weld metal interface) regions of ex-service 2-1/4Cr-1Mo steels have been developed previously.[8] The *J-R* curves of these materials are compared with the present results in the base and HAZ regions, as shown in Figures 11(a) and (b). Figure 11(a) shows the data points of the *J-R* curves of the base, weld, HAZ, and fusion line metals, while Figure 11(b) presents the data bands. The base metals generally exhibited higher levels of *J-R* curves than the weld, HAZ, or fusion line metals. Increasing crack extension increased the

Table III. Tensile Properties of 2-1/4Cr-1Mo Steel

Specimen Number	Material Type	Location	Temperature, °C	Yield Strength, MPa	Ultimate Tensile Strength, MPa	Elongation,** Pct	Reduction in Area, Pct	D, MPa^{-m}	m
WCB-T3	base	cold region	− 40	201	435	34.8	72.2	2.21×10^{-12}	4.01
WCB-T4	base	cold region	− 40	205	443	31.8	76.2	1.03×10^{-11}	3.76
WHB-T1	base	hot region	593	135	209	31.5	73.3	4.51×10^{-12}	4.34
WHB-T2	base	hot region	593	126	197	32.1	72.0	1.39×10^{-13}	4.99
WCB-T1	base	cold region	593	106	192	55.5	76.8	2.49×10^{-11}	4.11
WCB-T2	base	cold region	593	105	185	35.9	72.9	6.97×10^{-14}	5.24
WCW-T1H*	HAZ	cold region	593	121	189	31.1	67.6	9.74×10^{-13}	4.65
WCW-T2H*	HAZ	cold region	593	117	160	29.4	48.8	3.56×10^{-15}	5.91

*Using a composite specimen with the HAZ area at the center of the gage length section.
**The gage length of the extensometer equaled 20.3 mm.

difference in the *J-R* curves between the base and the weld (HAZ or fusion line) materials. The levels of *J-R* curves of the weld, HAZ, and fusion line materials were found to be essentially comparable. Note that the *J-R* curves in the present HAZ regions were located within the scatter bands of the *J-R* curves in the previous fusion line areas.

2. *Fracture toughness*

The values of initiation toughness, J_{IC}, determined from the fracture toughness tests on the 2-1/4Cr-1Mo steel are presented in Table IV. The values of K_{Ji} are also listed for reference, which were determined from the following relationship with J_{IC}:

$$K_{Ji} = \left(\frac{J_{IC} E}{1 - \nu^2} \right)^{1/2}$$

where E is Young's modulus and ν is Poisson's ratio.

Some scatter in the J_{IC} values of the duplicate tests at 593 °C was found for one of the base metals (cold region) and also in the HAZ specimens (cold region). This trend was consistent with the variability observed in the two regions, as shown in Figure 10. The average values of fracture toughness (J_{IC}) for the hot and cold regions of the base metal and the HAZ (cold region) were 160, 185, and 153 kJ/m^2, respectively. Recently, the values of J_{IC} in the fusion line area of an ex-service 2-1/4Cr-1Mo steel weldment at 538 °C were determined to vary from

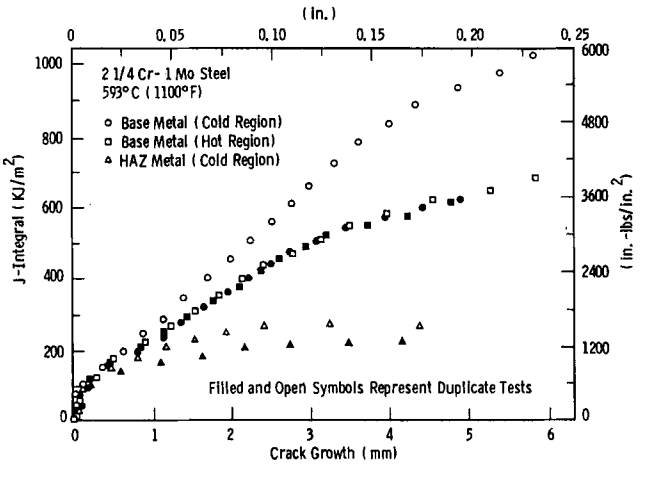

Fig. 10—Comparison of *J-R* curves of the base metals (hot and cold regions) and the HAZ metals of 2-1/4Cr-1Mo steel at 593 °C (1100 °F).

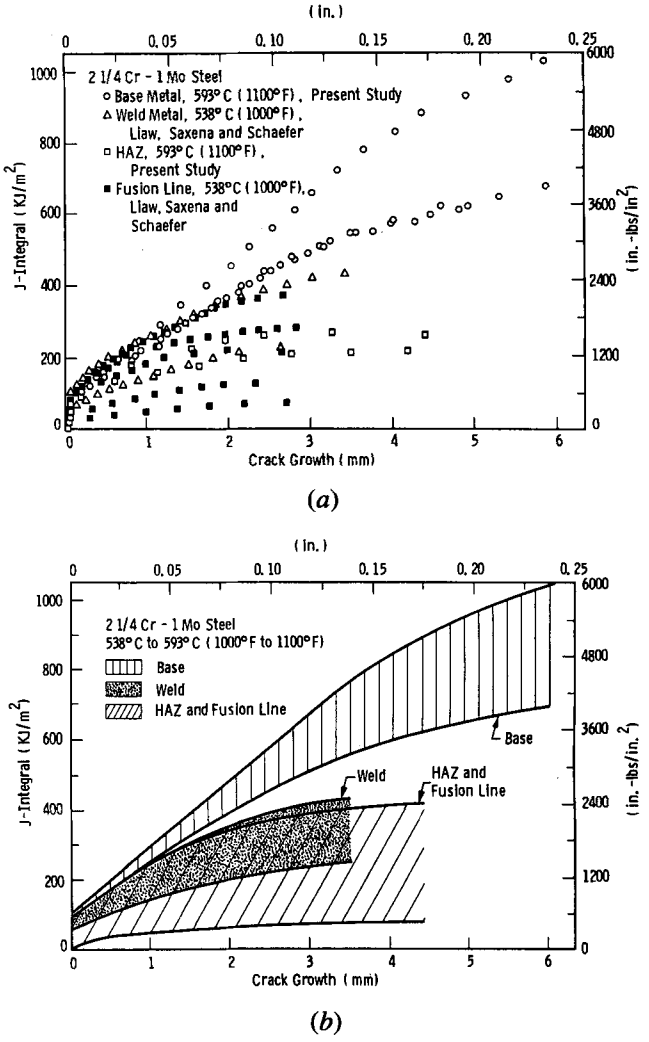

Fig. 11—Comparison of (*a*) *J-R* curves and (*b*) *J-R* curve data bands of the base, weld, HAZ, and fusion line metals of 2-1/4Cr-1Mo steel.

Table IV. Fracture Toughness Results of 2-1/4Cr-1Mo Steel

Specimen Number	Material Type	Location	Temperature, °C	J_{IC}, kJ/m^2	K_{Ji}, MPa$\sqrt{m}$	Tearing Modulus, T	θ,** Degree	$[K_{1i}^2(\theta) + K_{2i}^2(\theta)]^{1/2}$
WCB1A-J3	base	cold region	− 40	111*	—	—	~ 0	~1
WCB1A-J4	base	cold region	− 40	602*	—	—	~ 0	~1
WHB1-J1	base	hot region	593	159	183	940	~ 0	~1
WHB1-J2	base	hot region	593	163	187	954	~ 0	~1
WCB1A-J1	base	cold region	593	159	166	1030	~ 0	~1
WCB1A-J2	base	cold region	593	213	192	1389	34.8	0.910
WCW1A-J1H	HAZ	cold region	593	139	165	312	40.4	0.880
WCW1A-J2H	HAZ	cold region	593	168	181	507	51.9	0.808

*Maximum J before failure.
**θ is the crack deflection angle.

31 to 204 kJ/m^2.[8] The present fracture toughness results in the HAZ area seemed to be within the range reported previously.[8] This trend is consistent with the results presented in Figure 11.

At −40 °C, the fracture toughness tests were not valid in accordance with the ASTM Test Standard,[15] and thus, the maximum J values before failure for the duplicate tests are listed in Table IV. A significant scatter in the maximum J values was observed. This behavior is typical of fracture toughness results in the transition region, as will be discussed later.

At 593 °C, the base metals machined from hot and cold regions seemed to exhibit comparable toughness with the exception of the result from one test in the cold region. The unusually high J_{IC} value from that test was due to out-of-plane crack growth (crack deflection) and will be discussed later. The J_{IC} values of the base metal regions were approximately 20 pct higher than those of the HAZ (cold region).

The value of tearing modulus (T)[21] is also included in Table IV. T is defined as follows:

$$T = \frac{E}{\sigma_f^2}\frac{dJ}{da}$$

where E is Young's modulus, σ_f (flow stress) = 1/2 (σ_y + σ_u), σ_y is yield strength, σ_u is ultimate tensile strength, and dJ/da is the slope of the least-squares line between the two exclusion lines in the J-integral *vs* crack extension curve (the J-R curve).[15] The higher the tearing modulus, the greater the ability of a material to absorb energy upon additional crack extension. The values of T in the base metals were found to be much higher than those in the HAZ. This trend suggests that the base metal is more stable against tearing mechanisms during crack extension than the HAZ.

E. *Characterizations of Microscopic Aspects of Fracture*

After the fracture toughness tests were completed, the specimens were sectioned, polished, and etched along the crack growth direction to reveal the crack profiles. The fracture surfaces of selected specimens were examined by SEM. Results from these studies are described below.

1. *Crack profile*

It is of considerable interest to determine the fracture path in the HAZ fracture specimens with respect to the base metal/weld metal interface. In addition, some insight regarding the data scatter in fracture toughness properties of duplicate specimens can be gained by observing the fracture profiles.

Figure 12 shows the crack profile of one of the duplicate tests using the composite CT 2-1/4Cr-1Mo steel specimens (WCW1A-J1H and WCW1A-J2H) tested at 593 °C. The initial notch in the specimen was accidentally machined in the base metal region. Thus, the fatigue precrack extended in the base metal. Interestingly, during fracture toughness testing, the crack deflected from the base metal area into the HAZ area.

To quantify the extent of crack deflection, the angle of deflection (θ) was measured and listed in Table IV for specimens WCW1A-J1H and J2H. The value of θ is defined as the angle between the deflected crack and the original crack plane, as shown in Figure 13. It was found that θ in specimen WCW1A-J2H was greater than that in specimen WCW1A-J1H. This trend indicated that the extent of crack deflection in specimen WCW1A-J2H was more significant than that in specimen WCW1A-J1H.

The greater extent of crack deflection in specimen WCW1A-J2H than in specimen WCW1A-J1H corresponded to the higher level of J-R curve and the greater fracture toughness (J_{IC} or K_{IC}) in WCW1A-J2H, as shown in Table IV and Figure 10. Crack deflection typically reduced the crack driving force.[22–27] Thus, at an equivalent crack length, the deflected crack generally required more driving force to extend the crack than a nondeflected crack. Consequently, the levels of J-R curves and the values of fracture toughness were greater for the deflected crack, as compared to the nondeflected crack[22] (Table IV and Figure 10), as detailed in the Appendix.

Moreover, in the stable crack growth region of the composite CT specimen, the crack deflected from the base metal area into the HAZ area, as mentioned previously. This behavior indicated that during fracture toughness testing, the resistance to crack extension in the HAZ area was inferior to that in the base metal. This trend was also in agreement with the lower levels of J-R curve and fracture toughness in the HAZ than in the base metal, as shown in Figure 10.

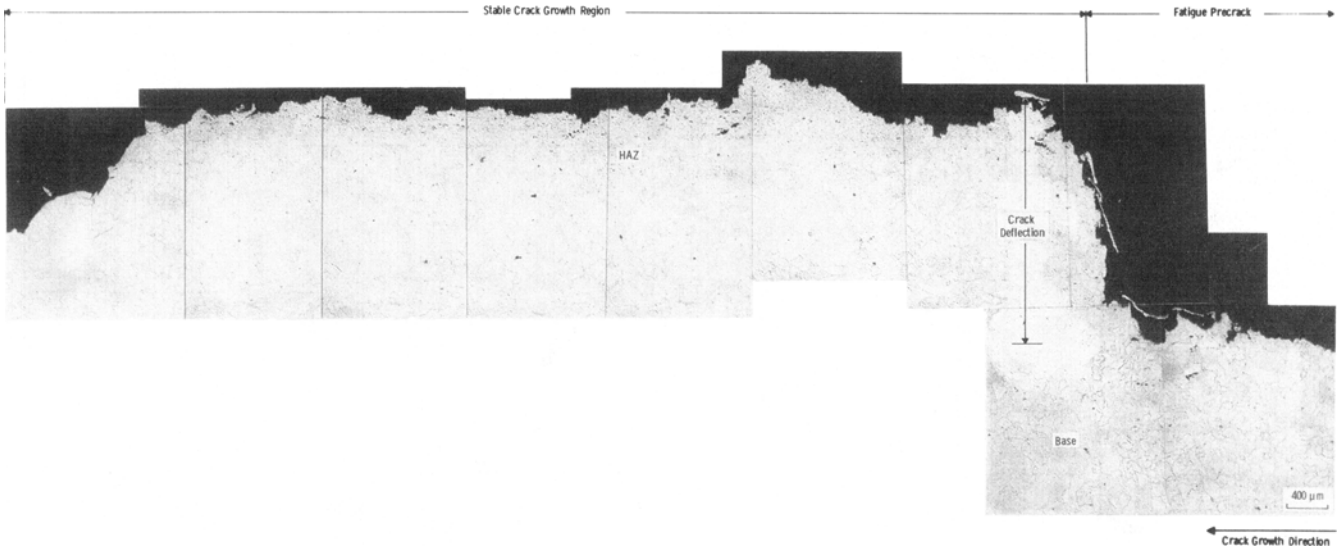

Fig. 12—Fracture profile of 2-1/4Cr-1Mo steel weldment (HAZ metal: specimen WCW1A-J2H) tested at 593 °C (1100 °F).

For the duplicate tests [specimens WCB1A-J1 and WCB1A-J2 (Table IV)] on the base 2-1/4Cr-1Mo steel (cold region), the fracture profile of specimen WCB1A-J2 exhibited a greater extent of crack deflection than that of specimen WCB1A-J1. Consistently, a greater θ value in specimen WCB1A-J2 than in the specimen WCB1A-J1 was found in Table IV. This trend is in agreement with the higher level of J-R curve and the greater J_{IC} (or K_{IC}) in specimen WCB1A-J2 than in specimen WCB1A-J1 (Table IV and Figure 10). Further analysis on crack deflection can be found in the Appendix.

2. *Fractography*

The fracture surfaces of tested fracture toughness specimens were cleaned and examined using SEM. Fracture morphology of the 2-1/4Cr-1Mo steel is shown in Figures 14 and 15. Figure 14 presents the fracture mode of the base metal (cold region) tested at −40 °C, while Figures 15(a) and (c) show the fracture modes of the base metal (cold region) and the HAZ (cold region) tested at 593 °C, respectively. In addition, Figures 15(b) and (d) show the corresponding cross-sectional views of the fracture paths.

Beyond the fatigue precrack area, cleavage fracture was dominant at −40 °C, which was preceded by a limited amount of dimpled fracture (Figure 14). Thus, the fracture toughness value reported in Table IV may be in the lower transition region, which may be somewhat higher than the lower-shelf fracture toughness.

At 593 °C in the base metal, fracture characteristics were ductile, and dimpled fracture was the prime mode (Figure 15(a)). In the cross-sectional view, ductile profiles were also observed (Figure 15(b)). In the HAZ, initial observations suggested that a dimpled rupture fracture mode was dominant for the HAZ specimen. However, detailed examination of the fracture surface revealed the mixed-mode fracture, *i.e.*, the presence of some regions

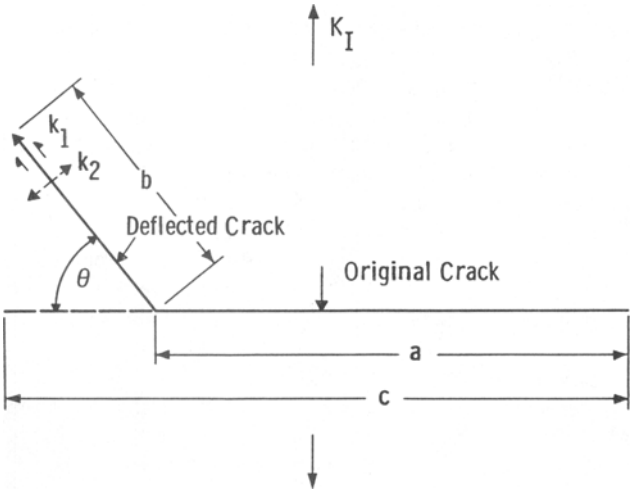

Fig. 13—Definition of crack deflection angle (θ).

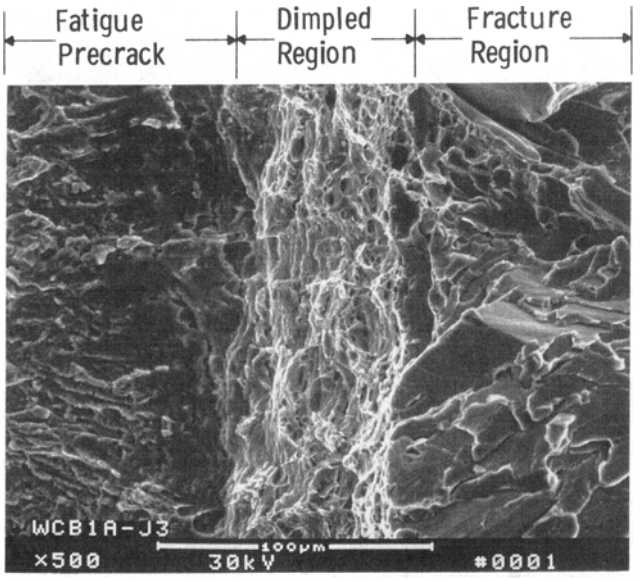

Fig. 14—Fracture morphology of 2-1/4Cr-1Mo steel [base metal (cold region)] at −40 °C (−40 °F).

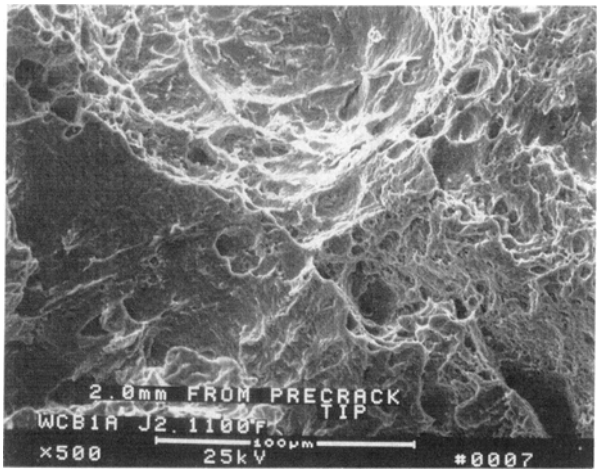

(*a*) Fractograph of Base Metal (Cold Region)

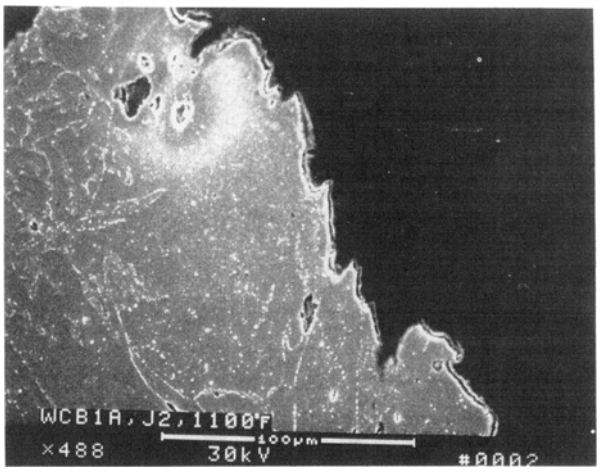

(*b*) Cross-section View of Base Metal (Cold Region)

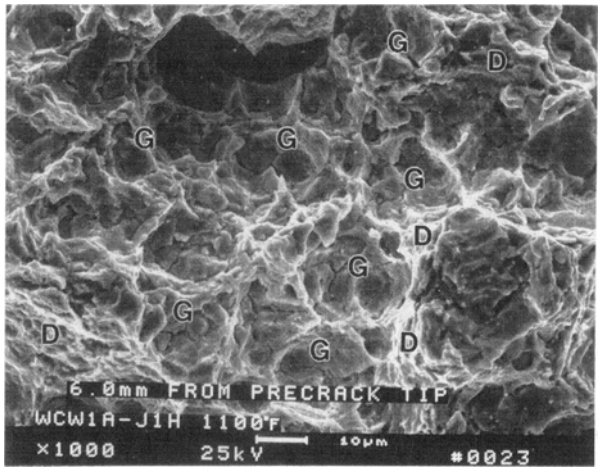

(*c*) Fractograph of HAZ Metal (Cold Region)

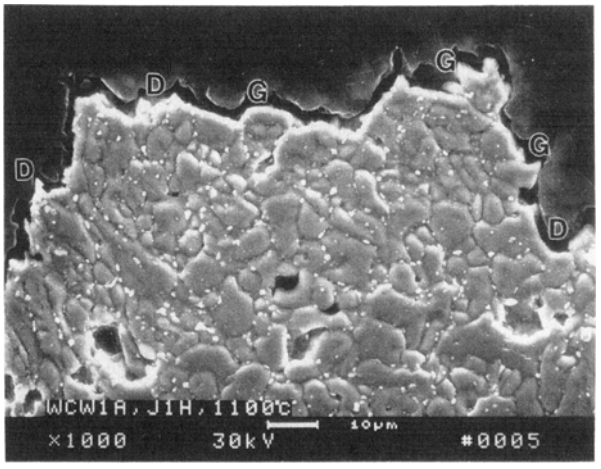

(*d*) Cross-section View of HAZ Metal (Cold Region)

Fig. 15—SEM fractographs and corresponding cross-sectional microstructures for 2-1/4Cr-1Mo steel tested at 593 °C: (*a*) and (*b*) base metal, and (*c*) and (*d*) HAZ samples. "Granular" and dimpled rupture regions on the HAZ fracture surface and the corresponding cross-sectional photographs are labeled "G" and "D," respectively.

which consisted of fine (~1- to ~3-μm diameter) microvoids and areas which exhibited a "granular" morphology (~8- to ~10-μm diameter). These regions were not observed in the base metal specimens tested at 593 °C. The fine size of these "granular" regions suggests that they are related to the microstructure of the HAZ, which consisted of ~6 to ~10 μm fine ferrite grains (Figures 4 and 5). Examination of cross-sectional specimens prepared from the fracture surfaces confirmed the presence of "granular" regions in the HAZ (Figure 15(d)). Note that SEM fractographs and cross-sectional microstructures are presented in Figures 15(c) and (d), respectively. "Granular" regions are labeled "G," whereas areas of dimpled rupture are labeled "D."

The mixed-mode fracture in the HAZ area resulted in the lower *J-R* curve, J_{IC}, and tearing modulus, as compared to the base metal (Table IV and Figure 10). In contrast, the ductile dimpled fracture in the base metal gave the higher fracture toughness resistance, relative to that in the HAZ. Moreover, the lower fracture toughness in the HAZ is also accompanied with the increase in hardness and strength,[11,12] relative to the base metal.

F. *Effect of Microstructure on Fracture Behavior*

Although agglomerated intergranular carbides were observed in both HAZ and base metal of the 2-1/4Cr-1Mo steel, the proportion of the grain boundary covered by these carbides in the HAZ was greater than that of the base metal (Figures 4 through 7). Particularly, the ratio of intergranular carbide size to grain size in the HAZ was much greater than that in the base metal. These trends indicate that the "granular" fracture morphology in the HAZ area of the 2-1/4Cr-1Mo steel (Figures 15(c) and 15(d)) is related to the presence of large carbides along the grain boundaries. (Figures 4 and 5).[28–33] The fine

"granular" fracture morphology is correlated to the fine ferrite grain size and extensive carbide coverage of the grain boundaries. In particular, the fine ferrite grain size [decorated by carbides in Figures 4 and 5 (TEM photographs)] was comparable to the "granular" fracture morphology (Figure 15(d)). This trend further confirmed the presence of "granular" failure in the HAZ. The observed fracture morphology is not unexpected in that the brittle carbides present on the grain boundaries can provide an easy fracture path. Furthermore, it is also known that localized strain[34] and potential grain boundary segregation of tramp elements, such as phosphorus, sulfur, and tin (along the grain boundaries where the extent of carbide precipitation is extensive), will promote "granular" fracture.[18,29,35–39] Thus, the presence of "granular" fracture in the HAZ resulted in lower fracture toughness, as compared to the base metal.

IV. CONCLUSIONS

1. The levels of *J-R* curves in the HAZ were found to be lower than those in the base metals of the ex-service 2-1/4Cr-1Mo steel. Correspondingly, the values of fracture toughness in the HAZ were lower than those in the base metals.
2. Dimpled fracture was characteristic of the fracture mode in the base metal, while brittle fracture (*e.g.*, "granular" fracture) mixed with ductile dimples was the prevalent fracture mode in the HAZ.
3. The lower *J-R* curve in the HAZ than in the base metal was related to the presence of "granular" fracture in the HAZ.
4. In HAZ, the presence of the "granular" fracture morphology was related to the fine grain size and the dense accumulation of carbides along the grain boundaries.
5. The variability in the *J-R* curves of both base and HAZ metals correlated with the extent of crack deflection.

APPENDIX

Analysis of Fracture Toughness of Deflected Crack

Generally, two local Mode I and Mode II stress intensities (k_1 and k_2) can be used to characterize the driving force of a deflected crack[40] (Figure 13). For a crack with a deflection angle (θ) subjected to nominal Mode I applied loading (Figure 13), the values of k_1 and k_2 were of the form[40]

$$k_1 = K_{11}(\theta)\, K_I \qquad [A1]$$

$$k_2 = K_{21}(\theta)\, K_I$$

where K_I is the stress intensity factor corresponding to the Mode I crack (Figure 13).

$$K_{11}(\theta) = \cos^3\left(\frac{\theta}{2}\right) \qquad [A2]$$

$$K_{21}(\theta) = \sin\left(\frac{\theta}{2}\right)\cos^2\left(\frac{\theta}{2}\right)$$

In Figure 13, a and b are the original and deflected crack lengths, respectively, while c is the total projected crack length. The value of K_I in Eq. [A1] should be calculated based on the projected length (c). Moreover, Eqs. [A1] and [A2] are effective for a deflected crack only when $a \gg b$. In this investigation, the value of a was much greater than b, as shown in Figures 1(b) and 12.

The effective stress intensity factor, K_{eff}, for a deflected crack can be defined as[41,42]

$$K_{eff} = (k_1^2 + k_2^2)^{1/2}$$

$$= [K_{11}^2(\theta) + K_{21}^2(\theta)]^{1/2} K_I \qquad [A3]$$

For a plane-strain, small-scale yielding condition,[40,41]

$$J_{eff} = (1 - \nu^2)\frac{K_{eff}^2}{E} = \frac{(1 - \nu^2)}{E}$$

$$\cdot [K_{11}^2(\theta) + K_{21}^2(\theta)]\, K_I^2 \qquad [A4]$$

where J_{eff} is the effective J integral for a deflected crack.

For a deflected crack, the failure is assumed to occur when an effective toughness, $J_{IC,eff}$ (or $K_{Ji,eff}$), is reached at the crack tip. In Eq. [A4], the value of J_{eff} (or K_{eff}) is set at $J_{IC,eff}$ (or $K_{Ji,eff}$), and K_I is the measured fracture toughness, K_{Ji}, corresponding to fracture for the deflected crack. Thus,

$$J_{Ji,eff}^{1/2} = \left[\frac{(1 - \nu^2)}{E}\right]^{1/2} K_{Ji,eff} = \left[\frac{(1 - \nu^2)}{E}\right]^{1/2}$$

$$\cdot [K_{11}^2(\theta) + K_{21}^2(\theta)]^{1/2} K_{Ji(\text{measured})} \qquad [A5]$$

In Eq. [A5], the value of K_{Ji} is inversely proportional to $[K_{11}^2(\theta) + K_{21}^2(\theta)]^{1/2}$ since $J_{IC,eff}$ (or $K_{Ji,eff}$) is a constant. The relationship between $[K_{11}^2(\theta) + K_{21}^2(\theta)]^{1/2}$ and θ is plotted in Figure A1. It was observed that as the extent of crack deflection increased (*i.e.*, the value of θ increased), $[K_{11}^2(\theta) + K_{21}^2(\theta)]^{1/2}$ decreased. Therefore, increasing the extent of deflection decreased the

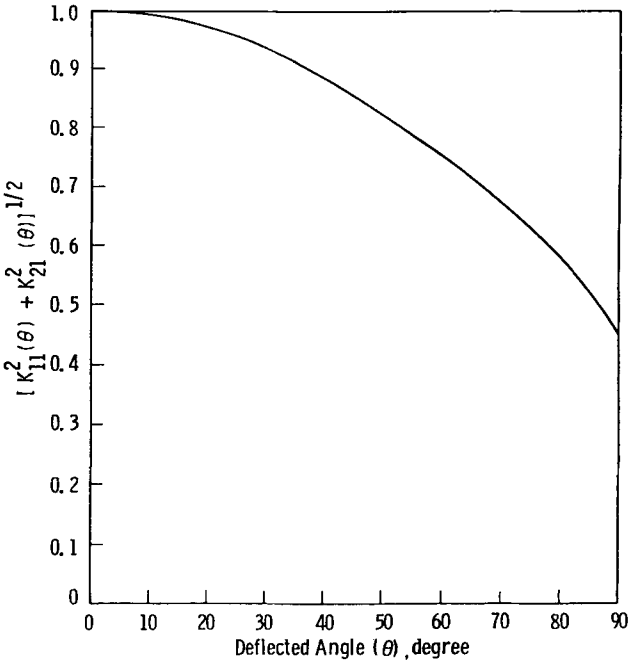

Fig. A1—Relationship between $[K_{11}^2(\theta) + K_{21}^2(\theta)]^{1/2}$ and θ.

Table AI. Values of $J_{IC,eff}$ and $K_{IC,eff}$

Specimen Number	Steel	Material Type	Location	Temperature, °C	J_{IC}, kJ/m^2	$J_{IC,eff}$, kJ/m^2	K_{Ji}, MPa$\sqrt{m}$	$K_{Ji,eff}$, MPa$\sqrt{m}$
WHB1-J1	2-1/4Cr-1Mo	base	hot region	593	159	159	183	183
WHB1-J2	2-1/4Cr-1Mo	base	hot region	593	163	163	187	187
WCB1A-J1	2-1/4Cr-1Mo	base	cold region	593	159	159	166	166
WCB1A-J2	2-1/4Cr-1Mo	base	cold region	593	213	176	192	175
WCW1A-J1H	2-1/4Cr-1Mo	HAZ	cold region	593	139	108	165	145
WCW1A-J2H	2-1/4Cr-1Mo	HAZ	cold region	593	168	109	181	146

value of $[K_{11}^2(\theta) + K_{21}^2(\theta)]^{1/2}$ and thus K_{Ji} (measured) (Eq. [A5]). This trend is in qualitative agreement with the experimental results (K_{Ji} or J_{Ic}) of the duplicate tests presented in Table IV.

Using Eq. [A5], the values of $J_{IC,eff}$ and $K_{Ji,eff}$ were determined for each pair of duplicate tests with deflected cracks and are listed in Table AI. In contrast with the results of J_{IC} (or K_{Ji}), $J_{IC,eff}$ (or $K_{Ji,eff}$) was essentially identical for the duplicate tests. Thus, the variability of J_{IC} (or K_{Ji}) of the duplicate tests is much reduced by using $J_{IC,eff}$ (or $K_{Ji,eff}$) (or by taking crack deflection into consideration).

Summarizing the above discussion and the results presented in Table AI, Eq. [A5] has been experimentally shown to be effective in evaluating the effect of crack deflection on fracture toughness. Moreover, the concept of crack deflection can be quantified to explain the variability in measured fracture toughness values (K_{Ji} or J_{IC}). However, further analytical work is needed to assess the influence of crack deflection on the entire *J-R* curve, where large-scale plastic deformation can occur.

Note that in Table AI, the values of $J_{IC,eff}$ (or $K_{Ji,eff}$) in the base metals were greater than those in the HAZ for the 2-1/4Cr-1Mo steel. Moreover, the values of $J_{IC,eff}$ of the base metals in the hot and cold regions were nearly identical.

ACKNOWLEDGMENTS

The technical assistance of J.J. Haugh, T. Mullen, M.G. Peck, B.J. Sauka, and P.M. Yuzawich is gratefully acknowledged. The authors thank W.G. Clark, Jr. for helpful discussion. The work was supported by the Electric Power Research Institute (EPRI) under Contract No. RP-2253-10; R.H. Ryder (General Atomics, San Diego, CA) and R. Viswanathan (EPRI) are the contract monitors.

REFERENCES

1. P.K. Liaw and A. Saxena: *Remaining-Life Estimation of Boiler Pressure Parts—Crack Growth Studies*, EPRI CS-4688, Project 2253-7, Final Report, July 1986.
2. *Proc. Electric Power Research Institute (EPRI) Conf. on Life Extension and Assessment of Fossil Plants*, sponsored by EPRI, Edison Electric Institute (EEI), ASME, and ASM, Washington, DC, June 2–4, 1986.
3. W.A. Logsdon, P.K. Liaw, A. Saxena, and V.E. Hulina: *Eng. Fract. Mech.*, 1986, vol. 25, p. 259.
4. A. Saxena, P.K. Liaw, W.A. Logsdon, and V.E. Hulina: *Eng. Fract. Mech.*, 1986, vol. 25, p. 289.
5. V.P. Swaminathan, N.S. Cheruvu, A. Saxena, and P.K. Liaw: *An Initiation and Propagation Approach for the Life Assessment of an HP-IP Rotor*, Proc. EPRI Conf. on Life Extension and Assessment of Fossil Plants, sponsored by EPRI, EEI, ASME, and ASM, Washington, DC, June 2–4, 1986.
6. P.K. Liaw, G.V. Rao, and M.G. Burke: *J. Mater. Sci. Eng.*, in press.
7. C.E. Jaske: *Chem. Eng. Prog.*, April 1987, p. 37.
8. P.K. Liaw, A. Saxena, and J. Schaefer: *Eng. Fract. Mech.*, 1989, vol. 32, p. 675.
9. P.K. Liaw, A. Saxena, and J. Schaefer: *Eng. Fract. Mech.*, 1989, vol. 32, p. 709.
10. N.S. Cheruvu: *Aging of CrMoV Steel*, IP 850777, Westinghouse Power Generation Division, Orlando, FL, 1987.
11. P.K. Liaw and J.D. Landes: *Metall. Trans. A*, 1986, vol. 17A, pp. 473-89.
12. P.K. Liaw and J.D. Landes: *Effects of Monotonic and Cyclic Prestrain on Fracture Toughness: A Summary*, ASTM STP 945, ASTM, Philadelphia, PA, 1988, pp. 622-46.
13. J. Fouldes: General Atomics, San Diego, CA, unpublished research, 1987.
14. *ASTM Book of Standards*, ASTM Standard E399-83, ASTM, Philadelphia, PA, 1987, vol. 03.01.
15. *ASTM Book of Standards*, ASTM Standard E813-87, ASTM, Philadelphia, PA, 1987, vol. 03.01.
16. P. Albrecht, W.R. Andrews, J.P. Gudas, J.A. Joyce, F.J. Loss, D.E. McCabe, D.W. Schmidt, and W.A. VanDerSluys: *J. Test. Eval.*, 1982, vol. 10, p. 245.
17. *ASTM Book of Standards*, ASTM Standard E1152-87, ASTM, Philadelphia, PA, 1987, vol. 03.01.
18. G.A. Clarke: *J. Test. Eval.*, 1980, vol. 8 (5), p. 213.
19. P.M. Yuzawich and C.W. Hughes: *J. Pract. Metallogr.*, 1978, vol. 15, p. 184.
20. M.G. Burke: Westinghouse Research & Development Center, Pittsburgh, PA, unpublished research, 1988.
21. P.C. Paris and R.E. Johnson: ASTM STP 803, ASTM, Philadelphia, PA, 1983, p. II-5.
22. S. Suresh, A.K. Vasudevan, M. Tosten, and P.R. Howell: *Acta Metall.*, 1987, vol. 35, p. 25.
23. S. Suresh and R.O. Ritchie: *Metall. Trans. A*, 1982, vol. 13A, pp. 1627-31.
24. G.T. Gray, J.C. Williams, and A.W. Thompson: *Metall. Trans. A*, 1983, vol. 14A, p. 421.
25. D.J. Alexander and I.M. Bernstein: *Proc. Strength of Metals and Alloys*, Montreal, Canada, Pergamon Press, Ltd., Oxford, United Kingdom, Aug. 1985, vol. 2, p. 1163.
26. K.T. Faber and A.G. Evans: *Acta Metall.*, 1983, vol. 31, p. 565.
27. P.H. Dauskardt, R.D. Pendse, and R.O. Ritchie: *Acta Metall.*, 1987, vol. 35, p. 2227.
28. C.L. Briant and S.K. Banerji: *Metall. Trans. A*, 1979, vol. 10A, p. 123.
29. J.P. Materkowski and G. Krauss: *Metall. Trans. A*, 1979, vol. 10A, pp. 1643-51.
30. S.K. Banerji, C.J. McMahon, Jr., and H.C. Feng: *Metall. Trans. A*, 1978, vol. 9A, pp. 237-47.
31. T. Lichtenberg, W.M. Garrison, and J.M. Hyzak: *Proc. Topical Conference on Ferritic Alloys for Use in Nuclear Energy Technologies*, TMS-AIME Nuclear Metallurgy Committee, Warrendale, PA, 1983, p. 365.
32. C.L. Briant and N. Lewis: *Mater. Sci. Technol.*, 1986, vol. 2, p. 34.

33. C.A. Hippsley, J.E. King, and J.F. Knott: *Advances in the Physical Metallurgy and Applications of Steels*, Liverpool, United Kingdom, Sept. 1981, The Metals Society, London, United Kingdom, p. 147.
34. T. Ogura and T. Masmumoto: *Trans. Jpn. Inst. Met.*, 1986, vol. 27, p. 757.
35. M. Sarikaya, A.K. Jhingan, and G. Thomas: *Metall. Trans. A*, 1983, vol. 14A, pp. 1121-33.
36. B.C. Edwards: *Interfacial Fracture in Alloy Steels*, Martinus Nishoff Publishers, The Hague, The Netherlands, 1982.
37. P. Dreig, D. Lonsdale, and P.E.J. Flewitt: *Met. Sci.*, 1982, vol. 16, p. 335.
38. R.O. Ritchie, J.F. Knott, and J.R. Rice: *J. Mech. Phys. Solids*, 1973, vol. 21, p. 395.
39. R.O. Ritchie and A.W. Thompson: *Metall. Trans. A*, 1985, vol. 16A, p. 233.
40. B. Cotterell and J.R. Rice: *Int. J. Fract.*, 1980, vol. 16, p. 155.
41. C.F. Shih: in *Fracture Analysis*, ASTM STP 560, ASTM, Philadelphia, PA, 1974, p. 187.
42. S. Suresh and C.F. Shih: *Int. J. Fract.*, 1986, vol. 30, p. 237.